J|A|C|S
ARTICLES
Published on Web 01/25/2007

Oxygen as a Paramagnetic Probe of Clustering and Solvent Exposure in Folded and Unfolded States of an SH3 Domain

Irina Bezsonova,[†,‡] Ferenc Evanics,[§] Joseph A. Marsh,[‡,||] Julie D. Forman-Kay,[‡,||] and R. Scott Prosser*[,§]

Contribution from the Department of Chemistry, University of Toronto, 80 St. George Street, Toronto, ON, Canada, M5S 1A8, Program in Molecular Structure and Function, Hospital for Sick Children, 555 University Avenue, Toronto, ON, Canada, M5G 1X8, Department of Chemistry, University of Toronto, UTM, 3359 Mississauga Road North, Mississauga, ON, Canada, L5L 1C6, and Department of Biochemistry, University of Toronto, 1 King's College Circle, Toronto, ON, Canada, M5S 1X8

Received July 19, 2006; E-mail: sprosser@utm.utoronto.ca

Abstract: The N-terminal SH3 domain of the *Drosophila* modular protein Drk undergoes slow exchange between a folded (F_{exch}) and highly populated unfolded (U_{exch}) state under nondenaturing buffer conditions, enabling both F_{exch} and U_{exch} states to be simultaneously monitored. The addition of dissolved oxygen, equilibrated to a partial pressure of either 30 atm or 60 atm, provides the means to study solvent exposure with atomic resolution via ^{13}C NMR paramagnetic shifts in $^{1}H,^{13}C$ HSQC (heteronuclear single quantum coherence) spectra. Absolute differences in these paramagnetic shifts between the F_{exch} and U_{exch} states allow the discrimination of regions of the protein which undergo change in solvent exposure upon unfolding. Contact with dissolved oxygen for both the F_{exch} and U_{exch} states could also be assessed through ^{13}C paramagnetic shifts which were normalized based on the corresponding paramagnetic shifts seen in the free amino acids. In the F_{exch} state, the ^{13}C nuclei belonging to the hydrophobic core of the protein exhibited very weak normalized paramagnetic shifts while those with greater solvent accessible surface area exhibited significantly larger normalized shifts. The U_{exch} state displayed less varied ^{13}C paramagnetic shifts although distinct regions of protection from solvent exposure could be identified by a lack of such shifts. These regions, which included Phe9, Thr12, Ala13, Lys21, Thr22, Ile24, Ile27, and Arg38, overlapped with those found to have residual nativelike and non-native structures in previous studies and in some cases provided novel information. Thus, the paramagnetic shifts from dissolved oxygen are highly useful in the study of a transient structure or clustering in disordered systems, where conventional NMR measurements (couplings, chemical shift deviations from random coil values, and NOEs) may give little information.

Introduction

A significant fraction of proteins either lack a stable folded structure altogether or possess regions which are intrinsically disordered under physiological conditions.[1−3] These intrinsically disordered regions often play a key role in cell signaling and both transcriptional and translational regulation via protein interactions.[2,4] Disorder provides a route for transient low affinity binding, recognition of multiple partners, potentially faster recognition and dissociation, and reduced protein lifetimes in the cell, all of which may contribute to rapid regulation and cell cycle control.[5,6] Disordered protein regions frequently possess fluctuating local and tertiary structure which may be critical to their function. Sites where such a transient structure is present in disordered proteins may guide interactions with a binding partner. Thus, information about the contacts and structural propensities within these states is important.

Due to the dynamic nature of disordered ensembles, their structural characterization represents a significant challenge. Methods such as far- and near-UV circular dichroism, small-angle X-ray scattering (SAXS), sedimentation analysis, and dynamic light scattering provide general information about the hydrodynamic properties of the protein and extent of structure. However, these methods lack specific information on the particular residues involved in the formation of a structure. Multidimensional NMR spectroscopy provides site-specific structural and dynamic characterization of disordered proteins in the form of deviations from random coil values of chemical shifts[7−11] and scalar couplings[12] indicative of secondary structure

[†] Department of Chemistry, University of Toronto.
[‡] Hospital for Sick Children.
[§] University of Toronto, UTM.
[||] Department of Biochemistry, University of Toronto.

(1) Dyson, H. J.; Wright, P. E. *Nat. Rev. Mol. Cell Biol.* **2005**, *6* (3), 197−208.
(2) Fink, A. L. *Curr. Opin. Struct. Biol.* **2005**, *15* (1), 35−41.
(3) Uversky, V. N. *Protein Sci.* **2002**, *11* (4), 739−756.
(4) Tompa, P.; Csermely, P. *FASEB J.* **2004**, *18* (11), 1169−1175.
(5) Uversky, V. N.; Oldfield, C. J.; Dunker, A. K. *J. Mol. Recognit.* **2005**, *18* (5), 343−384.
(6) Tompa, P. *FEBS Lett.* **2005**, *579* (15), 3346−3354.
(7) Wishart, D. S.; Sykes, B. D. *Methods Enzymol.* **1994**, *239*, 363−392.
(8) Neidigh, J. W.; Fesinmeyer, R. M.; Prickett, K. S.; Andersen, N. H. *Biochemistry* **2001** *40*, (44), 13188−13200.
(9) Fesinmeyer, R. M.; Hudson, F. M.; Olsen, K. A.; White, G. W. N.; Euser, A.; Andersen, N. H. *J. Biomol. NMR* **2005**, *33* (4), 213−231.

10.1021/ja065173o CCC: $37.00

propensities. Furthermore, residual dipolar couplings,[13,14] and long-range contacts observed from paramagnetic relaxation enhancement using spin labels,[15,16] and, in some cases, nuclear Overhauser effect (NOE) data provide insight into tertiary structure propensity. However, the differences between a transient structure and statistical coil may be quite subtle. Therefore, additional sensitive probes of solvent exposure can be very useful to highlight a transient structure or clustering in disordered domains.

The extent of contact with solvent on a residue-level basis may also be assessed by solution NMR techniques and used to study topologies of disordered proteins. These techniques commonly include hydrogen/deuterium exchange experiments, measurements of NOEs between solvent and residue,[17,18] or the observation of paramagnetic shifts or relaxation rates resulting from the addition of soluble paramagnetic agents.[19,20] Typical paramagnetic additives include hydroxy-TEMPO (TEMPO, 4-hydroxy-2,2,6,6-tetramethyl-4-hydroxy-2,2,6,6-tetramethylpiperidinooxy) or lanthanide chelates.[21,22] Such additives may show preferential interactions with specific residues or charged sites[21] thereby altering the delicate equilibrium of conformers in disordered proteins. Oxygen is preferred as a paramagnetic additive due to its small size and uncharged nature, suggesting that it will be less perturbing. Here, we utilize dissolved oxygen as a paramagnetic additive and measure ^{13}C paramagnetic shifts to study solvent exposure of backbone and side chain nuclei of a model disordered protein, the unfolded state of a marginally stable drkN SH3 domain. The results point toward key regions of the protein in the unfolded state which exhibit significant clustering or increased solvent protection relative to the folded state.

Paramagnetic effects from dissolved oxygen are readily observed via T_1 and T_2 relaxation enhancement, which is significant at partial pressures of 20 atm or more for high-gamma nuclei[23−27] such as ^1H and ^{19}F. Such pressures are expected to give rise to minimal perturbations in protein conformation and can in any case be accounted for by control experiments under pressurized helium, as was routinely done in the current study. Moreover, paramagnetic relaxation rates are relatively easy to interpret in terms of protein surface structure and solvent exposure partly because the oxygen electronic spin relaxation times are sufficiently short to render the effective correlation time associated with modulation of the dipolar interaction constant.[28,29] However, paramagnetic relaxation rate analyses may be complicated by nonexponential relaxation or spin-diffusion effects in the absence of extensive deuteration of the protein. Alternatively, paramagnetic effects from dissolved oxygen may be directly observed from paramagnetic shifts of the ^{13}C resonances. In this case, solvent exposure on both the protein backbone and side chains may be probed. The use of chemical shift perturbations has the advantage that the effects are directly related to local oxygen concentrations, while one need not be concerned with deuteration levels and the effects of spin diffusion. Very small ^1H chemical shift perturbations from oxygen have been previously reported in protein studies,[30] and oxygen-induced ^{19}F chemical shift perturbations as high as 4.0 ppm at 100 atm oxygen partial pressures have been reported and used to study membrane immersion depth[31] and protein topology.[32] In the present case, we observe significant ^{13}C paramagnetic shifts (roughly 0.4 ppm or less) at oxygen partial pressures of 30 atm and 60 atm, which we interpret in terms of protein structure and solvent exposure, highlighting the particular utility of ^{13}C as a probe relative to ^1H. At such partial pressures, line broadening is relatively weak while the shifts, which have been previously attributed to a contact mechanism,[33] are sufficiently small that assignments are straightforward to make, particularly if spectra are recorded as a function of oxygen partial pressure.

Contact shifts ($\Delta\delta$), which arise from unpaired electron spin density at the resonant nucleus, have been previously considered in situations where the paramagnet was complexed with the protein.[19,34] In the present case of a freely diffusible paramagnet we adopt an empirical approach and assume the paramagnet does not undergo strong binding at or near the nucleus of interest, in which case the key variables should involve the local oxygen concentration, $\langle[O_2]\rangle_{local}$, and a collisionally accessible surface area, $\langle\Omega\rangle$. We also consider the possibility that the effect of a diffusible paramagnet may be different on sp^1-, sp^2-, or sp^3-hybridized carbon nuclei. This could arise due to differences in delocalization or polarizability, which we expect due to differences in aromaticity or p-orbital content. Therefore, we describe the shift in terms of the concentration and solvent exposed surface such that

$$\Delta\delta_{O_2} = k\alpha\langle\Omega\rangle\langle[O_2]\rangle_{local} \quad (1)$$

where k represents a proportionality constant and α represents a polarization or spin-delocalization term. This approach is somewhat similar to that adopted recently by Teng et al.[29] in

(10) Fong, S.; Bycroft, M.; Clarke, J.; Freund, S. M. V. *J. Mol. Biol.* **1998**, *278* (2), 417−429.
(11) Korzhnev, D. M.; Neudecker, P.; Mittermaier, A.; Orekhov, V. Y.; Kay, L. E. *J. Am. Chem. Soc.* **2005**, *127* (44), 15602−15611.
(12) Hennig, M.; Bermel, W.; Spencer, A.; Dobson, C. M.; Smith, L. J.; Schwalbe, H. *J. Mol. Biol.* **1999**, *288* (4), 705−723.
(13) Bernado, P.; Bertoncini, C. W.; Griesinger, C.; Zweckstetter, M.; Blackledge, M. *J. Am. Chem. Soc.* **2005**, *127* (51), 17968−17969.
(14) Bernado, P.; Blanchard, L.; Timmins, P.; Marion, D.; Ruigrok, R. W. H.; Blackledge, M. *Proc. Natl. Acad. Sci. U.S.A.* **2005**, *102* (47), 17002−17007.
(15) Gillespie, J. R.; Shortle, D. *J. Mol. Biol.* **1997**, *268* (1), 158−169.
(16) Gillespie, J. R.; Shortle, D. *J. Mol. Biol.* **1997**, *268* (1), 170−184.
(17) Gemmecker, G.; Jahnke, W.; Kessler, H. *J. Am. Chem. Soc.* **1993**, *115* (24), 11620−11621.
(18) Hwang, T. L.; Mori, S.; Shaka, A. J.; vanZijl, P. C. M. *J. Am. Chem. Soc.* **1997**, *119* (26), 6203−6204.
(19) Bertini, I.; Luchinat, C.; Parigi, G. *Concepts Magn. Reson.* **2002**, *14* (4), 259−286.
(20) Bertini, I.; Luchinat, C. *NMR of Paramagnetic Molecules in Biological Systems*; Benjamin-Cummings: Menlo Park, CA, 1986.
(21) Esposito, G.; Lesk, A. M.; Molinari, H.; Motta, A.; Niccolai, N.; Pastore, A. *J. Mol. Biol.* **1992**, *224* (3), 659−670.
(22) Niccolai, N.; Ciutti, A.; Spiga, O.; Scarselli, M.; Bernini, A.; Bracci, L.; Di Maro, D.; Dalvit, C.; Molinari, H.; Esposito, G.; Temussi, P. A. *J. Biol. Chem.* **2001**, *276* (45), 42455−42461.
(23) Teng, C. L.; Bryant, R. G. *J. Am. Chem. Soc.* **2000**, *122* (11), 2667−2668.
(24) Hernandez, G.; Teng, C. L.; Bryant, R. G.; LeMaster, D. M. *J. Am. Chem. Soc.* **2002**, *124* (16), 4463−4472.
(25) Teng, C. L.; Bryant, R. G. *Biophys. J.* **2004**, *86* (3), 1713−1725.
(26) Ellena, J. F.; Moulthrop, J.; Wu, J.; Rauch, M.; Jaysinghne, S.; Castle, J. D.; Cafiso, D. S. *Biophys. J.* **2004**, *87* (5), 3221−3233.
(27) Sakakura, M.; Noba, S.; Luchette, P. A.; Shimada, I.; Prosser, R. S. *J. Am. Chem. Soc.* **2005**, *127* (16), 5826−5832.
(28) Teng, C. L.; Hong, H.; Kiihne, S.; Bryant, R. G. *J. Magn. Reson.* **2001**, *148* (1), 31−34.
(29) Teng, C. L.; Hinderliter, B.; Bryant, R. G. *J. Phys. Chem. A* **2006**, *110* (2), 580−588.
(30) Ulmer, T. S.; Campbell, I. D.; Boyd, J. *J. Magn. Reson.* **2002**, *157* (2), 181−189.
(31) Prosser, R. S.; Luchette, P. A.; Westerman, P. W. *Proc. Natl. Acad. Sci. U.S.A.* **2000**, *97* (18), 9967−9971.
(32) Luchette, P. A.; Prosser, R. S.; Sanders, C. R. *J. Am. Chem. Soc.* **2002**, *124* (8), 1778−1781.
(33) Prosser, R. S.; Luchette, P. A. *J. Magn. Reson.* **2004**, *171* (2), 225−232.
(34) Bertini, I.; Castellani, F.; Luchinat, C.; Martini, G.; Parigi, G.; Ristori, S. *J. Phys. Chem. B* **2000**, *104* (45), 10653−10658.

which the paramagnetic relaxation rate acting on a given nucleus was expressed in terms of a local oxygen concentration and a steric term, f_k, describing the local accessibility of dissolved oxygen. The value of f_k could be computed over a lattice of excluded volume using an integral weighted by the inverse sixth power of the distance between the lattice site and the nucleus.[29] In contrast, the above steric term, $\langle\Omega\rangle$, is proposed to be shorter in range than f_k since delocalization or polarization effects are presumably collisionally mediated. An analysis of surface protons in the protein ribonuclease revealed that the average intermolecular free energy, ΔG°_k, associated with the interaction between oxygen and the protein surface protons was significant; $\Delta G^\circ_k/RT$ was found to vary between 0 and -3 with an average around -1.25.[29] Thus, the local oxygen concentration, $[O_2]_{local}$, cannot be neglected in the current analysis. In fact, $\Delta\delta_{O_2}$ gives some insight into the nature of the protein surface in terms of hydrophobicity. One way of accounting for the polarization or delocalization term, α, is to divide the measured chemical shift perturbation in the protein, $\Delta\delta_{O_2(prt)}$, by that observed for the equivalent ^{13}C species in the free amino acid, $\Delta\delta_{O_2(AA)}$, in which case the dominant terms of the normalized shift should simply involve the ratio of collisionally accessible surface areas and the ratio of local oxygen concentrations, giving

$$\Delta\delta^*_{O_2} \equiv \frac{\Delta\delta_{O_2(prt)}}{\Delta\delta_{O_2(AA)}} = \frac{\langle\Omega\rangle_{O_2(prt)}[O_2]_{prt}}{\langle\Omega\rangle_{O_2(AA)}[O_2]_{AA}}. \quad (2)$$

Thus, we expect this normalized shift ($\Delta\delta^*_{O_2}$) to represent a relative measure of solvent exposure and hydrophobicity, where in most cases variations in $\Delta\delta^*_{O_2}$ over a protein surface should be dominated by differences in solvent exposure. In principle, one could also interrogate each nucleus with a second paramagnetic shift reagent, X. Assuming the size of X was such that the collisionally accessible surface areas, $\langle\Omega\rangle_{X(prt)}$ and $\langle\Omega\rangle_{X(AA)}$, are comparable to their oxygen counterparts, then differences in the paramagnetic shifts, $\Delta\delta^*_{O_2}$, would arise from differential partitioning (i.e., $[X]_{prt}/[X]_{AA}$). The measurement of such paramagnetic shifts from two complimentary shift reagents, one hydrophilic and the other hydrophobic, would be anticipated to be useful in the study of the local surface potential, but this is beyond the scope of the current paper.

A model system that has been quite useful for development of techniques to characterize disordered states of proteins is the N-terminal SH3 domain of the *Drosophila* adapter protein Drk. Drk is a 23 kDa protein containing a central Src homology 2 (SH2) domain surrounded by two Src homology 3 (SH3) domains. Drk mediates signaling between receptor tyrosine kinases and *ras* G-proteins by the binding of its SH3 domains to proline-rich, hydrophobic regions of the guanine nucleotide exchange factor Sos.[35] SH3 domains, which are 50−70 residues in length, are found in a large number of proteins involved in signal transduction and cellular localization.[36,37] The isolated N-terminal SH3 domain of Drk (drkN SH3 domain) is marginally stable and exists in equilibrium between a folded (F_{exch}) and highly populated unfolded (U_{exch}) state under nondenaturing buffer conditions (50 mM phosphate buffer, pH 6.0),[38−41] with a ratio of folded-to-unfolded conformers close to 1:1 at 5 °C. The interconversion between the F_{exch} and U_{exch} states is slow on the NMR chemical shift time scale, giving rise to distinct resonances for each state, making the drkN SH3 domain an excellent model for the study of fluctuating structure in unfolded states, folding, and stability.

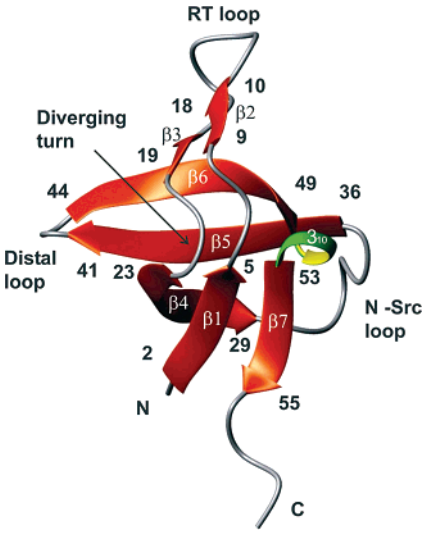

Figure 1. Three-dimensional structure of the folded state of the drkN SH3 domain (pdb ID 2A36). The residues at the N- and C-termini of various structural elements are labeled.

The folded state of the drkN SH3 domain, like other SH3 domains, forms a β-barrel or β-sandwich, as shown in Figure 1.[42] The U_{exch} state can be described as an ensemble of rapidly interconverting conformers. Previously reported NOE patterns and other structural data provide evidence for the presence of residual nativelike and non-native structures within the unfolded state ensemble.[39,41,43] Small-angle X-ray scattering and NMR diffusion measurements suggest that the U_{exch} state is compact, possessing an average radius of gyration about 30% larger than that of the F_{exch} state, versus a 60% larger radius expected for a random coil structure.[44] In unfolded, folding intermediate, and other disordered states, dynamic hydrophobic clustering or the fluctuating structure associated with hydrophobic residues is often observed, including small non-native hydrophobic clusters.[45−48] Some hydrophobic clusters and contacts between aromatics and hydrophobic residues in the drkN SH3 domain U_{exch} state have been identified by NOEs involving selectively protonated aromatics and δ-methyl protonated Ile and Leu residues in otherwise perdeuterated protein.[41]

(35) Barsagi, D. *Trends Endocrinol. Metab.* **1994**, *5* (4), 165−169.
(36) Musacchio, A.; Gibson, T.; Lehto, V. P.; Saraste, M. *FEBS Lett.* **1992**, *307* (1), 55−61.
(37) Musacchio, A.; Wilmanns, M.; Saraste, M. *Prog. Biophys. Mol. Biol.* **1994**, *61* (3), 283−297.
(38) Zhang, O. W.; FormanKay, J. D. *Biochemistry* **1997**, *36* (13), 3959−3970.
(39) Mok, Y. K.; Kay, C. M.; Kay, L. E.; Forman-Kay, J. *J. Mol. Biol.* **1999**, *289* (3), 619−638.
(40) Zhang, O.; Forman-Kay, J. D. *Biochemistry* **1995**, *34* (20), 6784−6794.
(41) Crowhurst, K. A.; Forman-Kay, J. D. *Biochemistry* **2003**, *42* (29), 8687−8695.
(42) Bezsonova, I.; Singer, A.; Choy, W. Y.; Tollinger, M.; Forman-Kay, J. D. *Biochemistry* **2005**, *44* (47), 15550−15560.
(43) Crowhurst, K. A.; Tollinger, M.; Forman-Kay, J. D. *J. Mol. Biol.* **2002**, *322* (1), 163−178.
(44) Choy, W. Y.; Mulder, F. A. A.; Crowhurst, K. A.; Muhandiram, D. R.; Millett, I. S.; Doniach, S.; Forman-Kay, J. D.; Kay, L. E. *J. Mol. Biol.* **2002**, *316* (1), 101−112.
(45) Smith, L. J.; Mark, A. E.; Dobson, C. M.; van Gunsteren, W. F. *J. Mol. Biol.* **1998**, *280* (4), 703−719.
(46) Kazmirski, S. L.; Wong, K. B.; Freund, S. M. V.; Tan, Y. J.; Fersht, A. R.; Daggett, V. *Proc. Natl. Acad. Sci. U.S.A.* **2001**, *98* (8), 4349−4354.
(47) Ragona, L.; Pusterla, F.; Zetta, L.; Monaco, H. L.; Molinari, H. *Folding Des.* **1997**, *2*, (5), 281−290.

In this study the drkN SH3 domain has been chosen as a model protein to assess possible applications of dissolved oxygen as a paramagnetic probe of solvent accessibility, particularly in disordered systems. Since a considerable body of structural information has been obtained on the U_{exch} ensemble, regions determined to be highly exposed or protected from dissolved oxygen in the U_{exch} state may be considered in terms of findings from prior structural studies including NMR experiments (NOEs, relaxation studies, hydrogen exchange experiments), fluorescence, and SAXS measurements.[38−41,43,44,49] In addition, data for the F_{exch} state can be derived at the same time, providing an internal control which may be compared to the folded state structure.[42] This paper explores the extent of solvent exposure of the drkN SH3 domain in its F_{exch} and U_{exch} states via ^{13}C chemical shift perturbations arising from dissolved oxygen as a paramagnetic contrast agent.

Materials and Methods

Free Amino Acid Samples. Each of 20 amino acids were obtained from Sigma Chemicals (Mississauga, ON). The amino acids were dissolved in 90/10 H_2O/D_2O containing 50 mM pH 6.0 sodium phosphate (intended to reproduce the pH used in the current protein study) and separated into six samples (Gly, Leu, Glu, and Trp in one sample; Gly, Ala, Pro, and Arg in the second sample; Gly, Val, Phe, and Lys in the third; Gly, His, Ile, Gln, and Tyr in the fourth; Gly, Ser, Asn, and Thr in the fifth; and Gly, Asp, Cys, and Met in the sixth sample) to avoid any spectral overlap in the $^1H,^{13}C$ HSQC (heteronuclear single quantum coherence) spectra. Most amino acid concentrations were on the order of several mg/mL and were adjusted to be well below their solubility limits. Chemical shifts for each amino acid were straightforward to measure and confirm with known shifts via ($^1H,^1H$) TOCSY spectra. Based on the chemical shifts observed in the absence of oxygen, there was no evidence of aggregation of any amino acids. Shifts associated with cysteine were not measured as the drkN SH3 domain has no cysteines and because cysteine has a propensity to oxidize or dimerize in the presence of significant concentrations of dissolved oxygen. Note that, in separate experiments of a protein possessing more than one exposed cysteine residue, we have observed that 50 mM concentrations of DTT (dithiothreitol) preserved the reduced state of cysteine for a week or more (data not shown). Each of the six samples contained Gly, which allowed us to account for slight differences in the degree of oxygenation among the different samples and rescale the shifts appropriately. Oxygenation levels were usually monitored by measuring the water T_1 relaxation time, and equilibration could be assessed by the lack of significant change in the lock signal. Aliphatic and aromatic HSQCs of the free amino acids were recorded at 5 °C and 600 MHz field strengths in the absence and presence of dissolved oxygen at an applied partial pressure of 30 atm. Paramagnetic shifts were then obtained by carefully comparing chemical shifts associated with the oxygenated and unoxygenated samples.

DrkN SH3 Domain Samples. All experiments on the drkN SH3 domain were performed at 5 °C on 0.8 to 1 mM ^{13}C, ^{15}N labeled protein samples in 50 mM phosphate buffer, pH 6.0 in the presence of 10% D_2O and 100 μM to 3 mM DSS (2,2-dimethyl-2-silapentane-5-sulfonate sodium salt), purified as described previously.[42] Side chain assignment experiments were recorded on a Varian Inova 500 MHz spectrometer. Aliphatic side chains of the drkN SH3 domain were assigned using a set of standard triple resonance experiments including CCC-TOCSY-NNH, HCC-TOCSY-NNH, and HCCH-TOCSY.[50] Aromatic side chain assignment was done using (Hβ)Cβ(CγCδ)Hδ and (Hβ)Cβ(CγCδCϵ)Hϵ 2D experiments.[51]

(^1H, ^{13}C) and ($^1H,^{15}N$) gradient selected HSQC two-dimensional experiments were performed at 5 °C on both 600 and 800 MHz Varian Inova spectrometers, using *z*-gradient equipped HCN triple resonance solution NMR probes. Spectra were referenced by first acquiring a one-dimensional ^1H NMR spectrum of the sample, containing 100 μM DSS, which was referenced to 0 ppm. To optimize resolution in the ^{13}C dimension, spectra were obtained from a sensitivity enhanced HSQC[52] for the aromatic region and a constant time (CT) HSQC[53] consisting of a 26.9 ms indirect dimension acquisition time for the aliphatic region. At 800 MHz, only aliphatic HSQCs, consisting of 16 scans and 408 increments in the indirect dimension, were obtained for both the unoxygenated sample and a sample under 30 atm of partial pressure of oxygen. To account for possible chemical shift perturbations arising purely from pressure, unoxygenated spectra were obtained after equilibrating the protein sample under equivalent partial pressures of helium. At 600 MHz, both aromatic and aliphatic HSQCs were recorded. The aliphatic HSQC consisted of 64 scans and 325 increments in the indirect dimension for both the unoxygenated sample and the sample at an oxygen partial pressure of 60 atm. The aromatic HSQC consisted of 16 scans and 400 increments in the indirect dimension for both the unoxygenated sample and the sample at an oxygen partial pressure of 60 atm. Typical 90° pulse lengths were 12.2 μs and 7.2 μs for ^{13}C and ^1H, respectively, and a homonuclear carbonyl decoupling pulse of 250 μs was used.

Oxygen Pressure. A 350 μL sample volume was deemed sufficient for shimming purposes, using a 5 mm OD, 3 mm ID sapphire NMR sample tube (Saint Gobain - Saphikon Crystals, Milford, NH), designed to tolerate pressures as high as 270 atm.[54] In principle, commercially available thick-walled NMR tubes can accommodate pressures as high as 60 atm (i.e., the highest pressure used in the present experiments). The sapphire tubes simply provide a slightly better filling factor than the glass counterparts. To measure effects of dissolved oxygen, samples were first equilibrated at 5 °C outside the magnet slightly above the desired oxygen partial pressure for 2 days and then equilibrated either overnight in the magnet (800 MHz) or for 2 days (600 MHz) at the desired partial pressure. Using open Swagelok connections (Swagelok, Solon, OH) to a pressurized oxygen supply, it was possible to maintain the pressure during the entire course of the NMR experiment.

Spectral Processing. All NMR data were processed using NMRPipe/NMRDraw[55] and analyzed with NMRView software.[56] In the case of the 600 MHz data, where spectral crowding was a more serious problem, the deconvolution program "FUDA"[57] was used to more accurately obtain peak positions. Typically, FIDs in the indirect dimension were first linear predicted to twice the number of points and subsequently apodized using a sine squared function, shifted by 0.4 radians. The standard deviations which were determined from the covariance matrix of the fit for ^{13}C and ^1H peak positions obtained from FUDA were estimated to be 0.0015 and 0.000 85 ppm, respectively.

Calculation of drkN SH3 Domain U_{exch} State Conformers. An initial conformer pool of 10 000 random structures with backbone dihedral angles distributed according to a GOR3[58] secondary structure prediction was generated with the program TraDES.[59] The program ENSEMBLE[60] was used with a Monte Carlo pseudo-energy minimiza-

(48) Koepf, E. K.; Petrassi, H. M.; Sudol, M.; Kelly, J. W. *Protein Sci.* **1999**, *8* (4), 841−853.
(49) Mok, Y. K.; Elisseeva, E. L.; Davidson, A. R.; Forman-Kay, J. D. *J. Mol. Biol.* **2001**, *307* (3), 913−928.
(50) Kanelis, V.; Forman-Kay, J. D.; Kay, L. E. *Iubmb Life* **2001**, *52* (6), 291−302.
(51) Yamazaki, T.; Forman-Kay, J. D.; Kay, L. E. *J. Am. Chem. Soc.* **1993**, *115* (23), 11054−11055.
(52) Palmer, A. G.; Cavanagh, J.; Wright, P. E.; Rance, M. *J. Magn. Reson.* **1991**, *93* (1), 151−170.
(53) Madsen, J. C.; Sorensen, O. W. *J. Magn. Reson.* **1992**, *100* (2), 431−436.
(54) Korzhnev, D. M.; Bezsonova, I.; Evanics, F.; Taulier, N.; Zhou, Z.; Bai, Y. W.; Chalikian, T. V.; Prosser, R. S.; Kay, L. E. *J. Am. Chem. Soc.* **2006**, *128* (15), 5262−5269.
(55) Delaglio, F.; Grzesiek, S.; Vuister, G. W.; Zhu, G.; Pfeifer, J.; Bax, A. *J. Biomol. NMR* **1995**, *6* (3), 277−293.
(56) Johnson, B. A.; Blevins, R. A. *J. Biomol. NMR* **1994**, *4* (5), 603−614.
(57) Kristensen, S. M. *Fuda: A function and data fitting and analysis package*; Chemistry Department, University of Copenhagen (smk@kiku.dk).

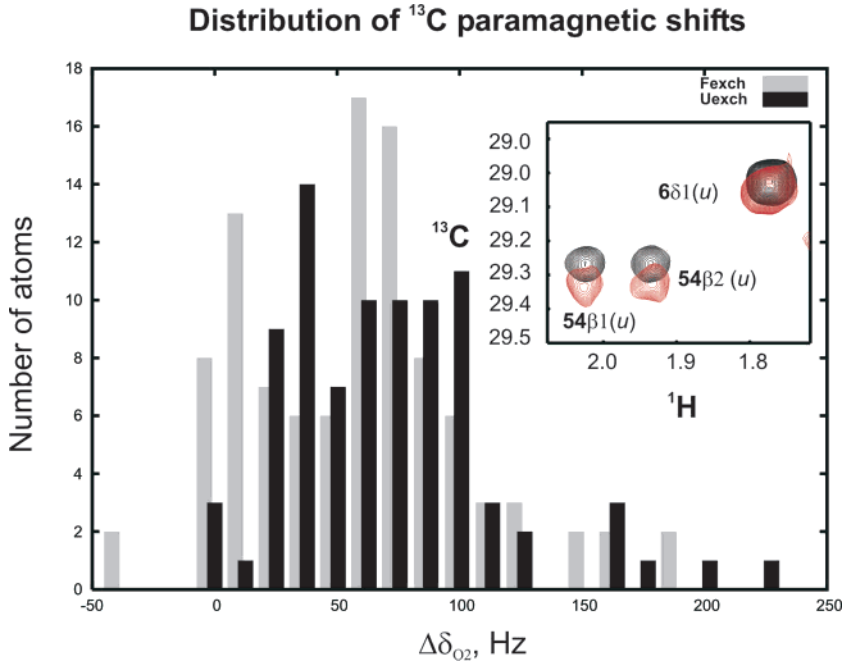

Figure 2. Distribution of paramagnetic shifts, $\Delta\delta_{O_2}$, arising from dissolved oxygen for the F_{exch} (gray bars) and U_{exch} (black bars) states of the drkN SH3 domain. A region of the ^{1}H, ^{13}C HSQC spectrum (at 600 MHz ^{1}H Larmor frequency) of the drkN SH3 domain recorded at 60 atm of helium (black) overlapped with the same region of the spectrum recorded under 60 atm of oxygen (red) is shown as an inset in order provide an example of the paramagnetic shifts observed. Note that the ^{13}C paramagnetic shifts are significantly greater than the corresponding ^{1}H paramagnetic shifts.

tion algorithm to select 40 structures from the initial conformer pool that are most consistent with a wide variety of experimental restraints. These included NOEs, *J*-couplings, ATCUN paramagnetic relaxation enhancements, solvent accessibility, and chemical shifts, essentially as was done previously[61] but without the hydrodynamic restraint (in order to enable selection of the more compact conformers in the ensemble). Random subsets of α-helical[39] and NOE restraints[42,60] were then applied to these structures in a dynamical annealing process using the program CNS[62] to generate 2000 derivative structures that are similar to those selected but which should be more consistent with experimental restraints. These new structures were combined with the original conformer pool, and ENSEMBLE conformer selection and CNS structure generation were repeated seven times. Finally, ENSEMBLE was used to select 10 structures from the entire conformer pool of 26 000 structures that collectively are most consistent with the experimental restraints.

Results

Contact Shift Measurements. Oxygen-induced ^{13}C chemical shift perturbations ($\Delta\delta_{O_2}$) were obtained from the difference between the ^{13}C resonances in the oxygenated and unoxygenated (^{1}H, ^{13}C) HSQC spectra of the drkN SH3 domain (Supporting Information Table S1). Due to the presence of the slowly exchanging F_{exch} and U_{exch} species in the NMR sample, these oxygen-induced ^{13}C paramagnetic shifts were simultaneously obtained for both states under exactly the same conditions. HSQC measurements were performed at 800 MHz at a partial pressure of 30 atm and at 600 MHz at a partial pressure of 60 atm. The paramagnetic shifts obtained at 800 MHz were found to be proportional to those observed at 600 MHz, which were approximately 2.5 times larger than those at 800 MHz due simply to the higher partial pressure and longer equilibration time. Using this scaling factor, *m*, data from both 800 and 600 MHz could be averaged to produce a consistent set of experimentally determined paramagnetic shifts as follows:

$$\Delta\delta_{O_2} = (m \times \Delta\delta_{800MHz} + \Delta\delta_{600MHz})/2. \quad (3)$$

The chi square value (0.82) associated with the fit also provides a measure of the reproducibility of the paramagnetic shift measurements which we estimate to be ±0.02 ppm, where shifts range from 0 to 0.4 ppm after equilibrating at 60 atm. A total of 101 paramagnetic shifts were obtained for the F_{exch} state (86 shifts for aliphatic resonances and 15 shifts for aromatics) while 85 paramagnetic shifts were obtained for the U_{exch} state (73 shifts for aliphatic resonances and 12 shifts for aromatics). The distribution of averaged paramagnetic shifts ($\Delta\delta_{O_2}$) are presented as a histogram for the F_{exch} state (shown in gray) and the U_{exch} state (shown in black) in Figure 2. The range of shifts observed, up to 0.4 ppm, demonstrates the utility of ^{13}C NMR shifts for exploring contact to dissolved oxygen. Note that the shift distribution associated with the F_{exch} state is slightly wider than that associated with the U_{exch} state which is expected since there is a distinct hydrophobic core and various layers of accessibility to water (and dissolved oxygen) in the folded state.

Comparison of Paramagnetic Shifts in the F_{exch} and U_{exch} States. The changes the protein undergoes upon folding (or unfolding) can be described by calculating the difference in paramagnetic shifts of the U_{exch} and F_{exch} states, which we define as

$$\Delta\Delta\delta_{O_2} \equiv \Delta\delta_{O_2}(U_{exch}) - \Delta\delta_{O_2}(F_{exch}). \quad (4)$$

(58) Brunger, A. T.; Adams, P. D.; Clore, G. M.; DeLano, W. L.; Gros, P.; Grosse-Kunstleve, R. W.; Jiang, J. S.; Kuszewski, J.; Nilges, M.; Pannu, N. S.; Read, R. J.; Rice, L. M.; Simonson, T.; Warren, G. L. *Acta Crystallogr., Sect. D* **1998**, *54*, 905−921.
(59) Garnier, J.; Gibrat, J. F.; Robson, B. *Methods Enzymol.* **1996**, *266*, 540−553.
(60) Choy, W. Y.; Forman-Kay, J. D. *J. Mol. Biol.* **2001**, *308* (5), 1011−1032.
(61) Marsh, J. A.; Neale, C.; Jack, F. E.; Choy, W.-Y.; Lee, A. Y.; Crowhurst, K. A.; Forman-Kay, J. D. *J. Mol. Biol.*, in press.
(62) Receveur-Brechot, V.; Bourhis, J. M.; Uversky, V. N.; Canard, B.; Longhi, S. *Proteins: Struct., Funct., Bioinf.* **2006**, *62* (1), 24−45.

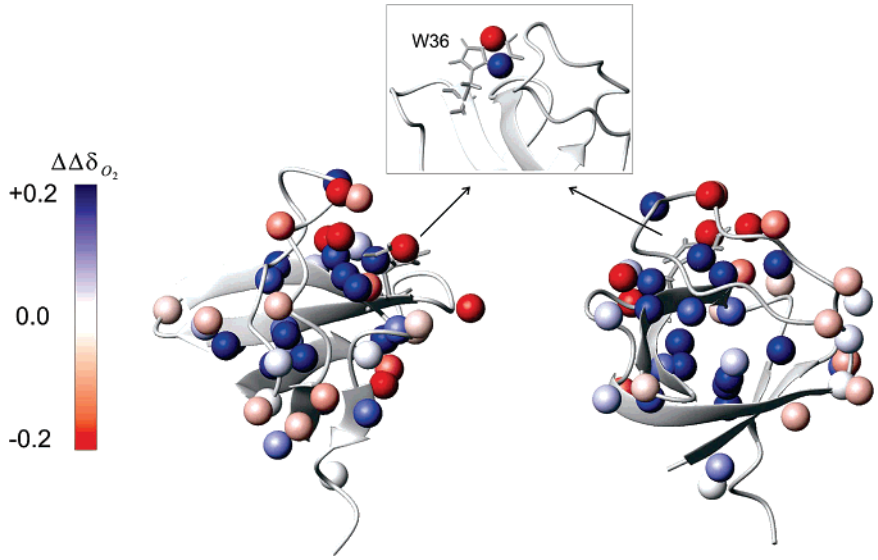

Figure 3. Difference in ^{13}C paramagnetic shifts between the U_{exch} and F_{exch} states [$\Delta\Delta\delta_{O_2} \equiv \Delta\delta_{O_2}(U_{exch}) - \Delta\delta_{O_2}(F_{exch})$] mapped onto the structure of the folded state, shown in two different orientations. The largest changes in the paramagnetic shifts are associated with atoms, indicated in blue, that are in the hydrophobic core of the F_{exch} state. Negative changes in paramagnetic shifts indicated in red are consistent with positions becoming more protected upon unfolding, possibly explained by non-native clusters in the U_{exch} state. The area around Trp36 is shown in the inset, demonstrating the asymmetry of the $\Delta\Delta\delta_{O_2}$ values for the aromatic ring.

Figure 3 maps $\Delta\Delta\delta_{O_2}$ onto the structure of the F_{exch} state, and values are listed in Supporting Information Table S2. Residues having the greatest changes ($\Delta\Delta\delta_{O_2} > 0$), indicative of greater solvent exposure upon unfolding, are highlighted in blue. These primarily include residues associated with the hydrophobic core of the F_{exch} state. The regions that do not experience significant change in the solvent exposure upon unfolding ($\Delta\Delta\delta_{O_2} = 0$) are indicated in white. Residues shown in red are in areas having decreased solvent exposure ($\Delta\Delta\delta_{O_2} < 0$) upon converting from the F_{exch} to the U_{exch} state. These might be associated with regions of non-native structure or clustering in the U_{exch} state since the native-like residual structure would be expected to have similar shifts in the two states. Here, we adopt the convention that those residues which are most protected in the U_{exch} state are indicated in the text by boldface, corresponding to red regions in Figure 3. Residues **Phe9**, **Thr12**, **Trp36**, **Leu47**, and Pro49, which are clustered in the F_{exch} state, all exhibit increased protection from solvent in the U_{exch} state. Ile4, Lys6, Asp8, Ser10, Arg20, Thr22, **Met30**, and **Ser34** also are clustered in the F_{exch} state and have increased solvent protection in the U_{exch} state.

Analysis of Solvent Exposure for the F_{exch} and U_{exch} States. We turn from a comparison of the paramagnetic shifts in the two states to a consideration of oxygen accessibility for the drkN SH3 domain in each of the F_{exch} and U_{exch} states. In the absence of a reference (i.e., the F_{exch} state) it is important to determine the possible influence of polarization or delocalization (i.e., α in eq 1) for certain types of carbon atoms in the protein. In addition, it is well-known that oxygen preferentially interacts with local hydrophobic pockets or regions of proteins associated with local free volume fluctuations,[25,29] and such preferential interactions may extend to individual carbon atoms in a given amino acid. With the intention of factoring out such weighting effects or preferential interactions between oxygen and different atoms in a given amino acid, we make use of the normalized shift, $\Delta\delta^*_{O_2}$, which is the measured paramagnetic shift, $\Delta\delta_{O_2}$, divided by the corresponding shift seen in the free amino acid, $\Delta\delta_{O_2(AA)}$.

Table 1 lists the observed paramagnetic shifts for various carbon atoms in 19 free amino acids. Note that the (^1H,^{13}C) HSQC spectra and corresponding shifts were obtained from six separate samples in order to minimize chemical shift overlap. Therefore, to account for slight differences in oxygenation, the raw shifts were first appropriately scaled based on the water T_1 under oxygen and the paramagnetic shifts observed for glycine, which was common to all samples. Ideally, a small tripeptide (e.g., GXG) might serve as a useful standard to obtain a better estimate of the paramagnetic shifts associated with a carbon in individual residues of a protein since the charges associated with the backbone amino and carboxyl groups of the free amino acid might well affect the oxygen interactions with nearby carbons, particularly the C_α. The paramagnetic shifts reported in Table 1 therefore represent a first approximation to amino acid specific reference ^{13}C paramagnetic shifts. Note that the paramagnetic shifts vary significantly across the table, which is somewhat surprising considering that the majority of the carbon atoms in the free amino acids are fully exposed to the solvent. A very weak correlation was found between the average paramagnetic shift for a given residue and the hydrophobicity using a variety of hydropathy scales (data not shown). Bryant and co-workers have pointed out that the extent of solvation, hydrophobicity, and local free volume all play a role in the specific interaction between oxygen and the local atoms.[25,29] Furthermore, polarization and delocalization effects may also scale paramagnetic shifts according to the type of carbon atom involved in the interaction with oxygen.

Figure 4A and B map the normalized paramagnetic shifts, $\Delta\delta^*_{O_2}$, of the F_{exch} and U_{exch} states of drkN SH3 onto the structure of the folded state of the drkN SH3 domain[42] with values listed in Supporting Information Table S1. Note that the largest normalized paramagnetic shifts in the F_{exch} state, shown

Table 1. Paramagnetic Shifts, $\Delta\delta_{O_2}$, from Free Amino Acids in the Presence of Dissolved Oxygen at a Partial Pressure of 30 atm

amino acid	atom	$\Delta\delta_{O_2}$ (ppm)	amino acid	atom	$\Delta\delta_{O_2}$ (ppm)
Ala	CA	0.049	Met	CB	0.066
Ala	CB	0.100	Met	CG	0.085
Arg	CA	0.037	Met	CE	0.132
Arg	CB	0.051	Phe	CA	0.063
Arg	CG	*a*	Phe	CB	0.051
Arg	CD	0.060	Phe	CG	*a*
Asn	CA	0.062	Phe	CD1/CD2	0.034
Asn	CB	0.052	Phe	CE1/CE2	0.070
Asp	CA	0.053	Phe	CZ	0.065
Asp	CB	0.065	Pro	CA	*a*
Gln	CA	0.043	Pro	CB	0.097
Gln	CB	0.067	Pro	CG	0.100
Gln	CG	0.063	Pro	CD	0.109
Glu	CA	0.045	Ser	CA	0.059
Glu	CB	0.069	Ser	CB	0.069
Glu	CG	0.077	Thr	CA	0.039
Gly	CA	0.080	Thr	CB	0.057
His	CA	*a*	Thr	CG2	0.071
His	CB	0.055	Trp	CA	*a*
His	CG	*a*	Trp	CB	0.054
His	CD2	*a*	Trp	CG	*a*
His	CE1	*a*	Trp	CD1	0.049
Ile	CA	0.046	Trp	CD2	*a*
Ile	CB	0.038	Trp	CE2	*a*
Ile	CG1	0.059	Trp	CE3	0.082
Ile	CG2	0.086	Trp	CZ2	0.058
Ile	CD1	0.098	Trp	CZ3	0.089
Leu	CA	0.032	Trp	CH2	0.089
Leu	CB	0.057	Tyr	CA	*a*
Leu	CG	0.017	Tyr	CB	0.062
Leu	CD1	0.086	Tyr	CG	*a*
Leu	CD2	0.087	Tyr	CD1/CD2	0.080
Lys	CA	0.053	Tyr	CE1/CE2	0.058
Lys	CB	0.038	Val	CA	0.065
Lys	CG	0.029	Val	CB	0.025
Lys	CD	0.041	Val	CG1	0.056
Lys	CE	0.077	Val	CG2	0.054
Met	CA	0.044			

[a] Data could not be obtained due to chemical shift overlap.

in blue in Figure 4A, arise exclusively from the protein exterior, while the smallest shifts, shown in red, are confined to a distinct region of the hydrophobic core. In contrast, the normalized paramagnetic shifts associated with the U_{exch} state (Figure 4B) do not reveal a distinct hydrophobic core, despite the fact that this compact unfolded state possesses an average radius of gyration that is only about 30% larger than that of the F_{exch} state.[44] However, there are clearly regions of solvent protected structure in the U_{exch} state as indicated by red clusters shown in Figure 4B.

The atoms in the U_{exch} state exhibiting some degree of protection from dissolved oxygen are identified with $\Delta\delta^*_{O_2}$ values less than 1.5 and are shown in Figure 4B. There are 19 such atoms arising from 17 residues: Met1 C_γ, Glu2 C_β, Asp 8 C_α, *Phe9* C_ζ, ***Thr12*** **C_α** and C_β, *Ala13* C_α, **Lys21 C_α**, *Thr22* C_α, *Ile24* C_α, Ile27 C_α, Met30 C_β, *Ser34* C_α, *Arg38* C_α, Ala39 C_α, Leu47 C_α, *Ser50* C_α and C_β, and Met55 C_α, where we again adopt the convention that the shifts exhibiting the greatest solvent protection in the U_{exch} state are indicated by boldface type while those residues which have been previously established to exhibit inter-residue NOEs in the U_{exch} state are italicized.

Discussion

Analysis of Paramagnetic Shift Data in the Context of Previous Structural Information for the U_{exch} State. The U_{exch} ensemble consists of rapidly interconverting conformers distinguished by residual nativelike and non-native structures.[39,41,43] In disordered proteins, including unfolded states and intrinsically disordered states, dynamic hydrophobic clustering or transient structure associated with hydrophobic residues, particularly tryptophans,[63] is often observed. Some hydrophobic clusters and contacts between aromatics and hydrophobic residues have been identified by NOEs involving selectively protonated aromatics and δ-methyl protonated Ile and Leu residues in otherwise perdeuterated drkN SH3 domain.[41] Evidence that the Trp36 indole has greater burial in the U_{exch} compared to F_{exch} state comes from stopped-flow fluorescence,[39] near-UV circular dichroism and hydrogen exchange NMR experiments.[43] Increased protection from solvent for the U_{exch} state in the vicinity of the indole group of Trp36 is also expected based on an abundance of NOE data showing that the tryptophan residue stabilizes a non-native hydrophobic cluster, centered around the indole group with long range aromatic-methyl NOEs involving Trp38 and Tyr37.[39,41] These hydrophobic residues may also include **Phe9**, **Leu47**, and Pro49, which have increased solvent protection as seen in Figure 3. Further evidence for the burial of the Trp36 indole was presented in a recent ^{19}F and ^1H NMR spectroscopic study of 5-fluorotryptophan substituted drkN SH3, which revealed that the indole group of Trp36 was relatively protected from the solvent in the U_{exch} state, while the 5-position was significantly exposed to the solvent.[64] This view of the asymmetry of the interaction of the Trp36 ring is seen in the inset of Figure 3, where the difference in paramagnetic shifts, $\Delta\Delta\delta_{O_2}$, shows a stark contrast in solvent exposure for the ^{13}C nuclei in the vicinity of the indole group and those furthest away from the indole on the six-membered ring of Trp36. In this case the side chain nuclei closest to the backbone appear to become more solvent exposed in the U_{exch} state while those near the indole group become more protected compared to their exposure in the F_{exch} state.

These results of asymmetry in oxygen accessibility associated with Trp36 in the U_{exch} state are corroborated by prior CLEANEX[18] NH exchange measurements with water, in which the backbone amide proton of Trp36 was shown to be relatively free to exchange with water while the indole proton was found to be significantly protected from solvent exposure in the U_{exch} state.[43] Such limited averaging in an otherwise very dynamic unfolded state ensemble is somewhat surprising and may be explained by formation of a hydrogen bond involving the Trp36 $N^{\epsilon 1}H$ as the proton donor. Tryptophan residues can participate in hydrogen bonds to backbone carbonyl groups via the indole protons in disordered systems, in a motif called the Trp-cage.[8,65] Additional support for the possibility of a Trp36 $N^{\epsilon 1}H$ hydrogen bond can be found in data for residue T22, which is found in a non-native helix extending from residues 18 to 26 that is stabilized by its interaction with both Trp36 and Tyr37 in the U_{exch} state. NOEs from Ser18 and Thr22 amides to the Trp36 $N^{\epsilon 1}H$ have been identified, confirming this interaction. In our study, Arg20 and Thr22, which belong to this non-native helix, show increased solvent protection in the U_{exch} relative to the F_{exch} state. The formation of this non-native structure is believed

(63) Klein-Seetharaman, J.; Oikawa, M.; Grimshaw, S. B.; Wirmer, J.; Duchardt, E.; Ueda, T.; Imoto, T.; Smith, L. J.; Dobson, C. M.; Schwalbe, H. *Science* **2002**, *295* (5560), 1719−1722.
(64) Evanics, F.; Kitevski, J. L.; Bezsonova, I.; Forman-Kay, J.; Prosser, R. S. *Biochie Biophys. Acta* **2006**.
(65) Barua, B.; Andersen, N. H. *Lett. Pept. Sci.* **2001**, *8* (3−5), 221−226.

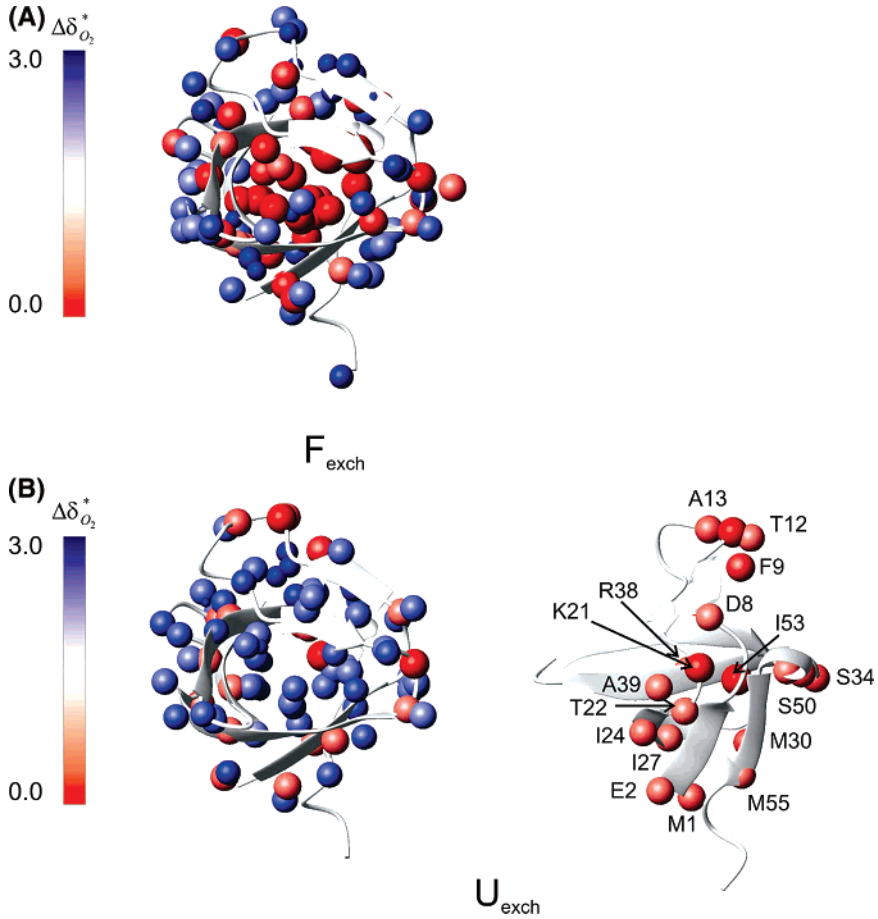

Figure 4. Normalized ^{13}C paramagnetic shifts, $\Delta\delta^*_{O_2}$, mapped onto the folded state structure for the (A) F_{exch} state and (B) U_{exch} state. A distinct subset of solvent protected locations is shown for clarity and labeled in the right panel of (B) in a different orientation. Shifts range from red (lowest, least solvent exposed) to blue (highest, most exposed). Note that $\Delta\delta^*_{O_2}$ is mapped using a common scale so that the F_{exch} and U_{exch} states can be compared directly.

to play a key role in the instability of the WT drkN SH3 domain. Mutation of Thr22 to glycine, in particular, disrupts non-native helical interactions in this region of the unfolded state, increasing its free energy and therefore forcing the equilibrium between the U_{exch} and F_{exch} states to be shifted toward the folded state.[49] Analysis of multiple mutants of Thr22 in the drkN SH3 domain revealed an inverse correlation between the maximum predicted α-helical propensity and the folding rate for the mutants[49] with outliers, including the wild type Thr22 and Ser22, that fold anomalously slowly. The explanation for the correlation is that the non-native helix in the unfolded state will slowly fold to the primarily β-sheet SH3 domain structure. Outliers are suggested to have a more stable helix structure than predicted based on the local sequence alone, due to tertiary contacts. Since both Thr22 and Ser22 have a hydroxyl group, these results hint at the possibility of a Trp36 $N^{\epsilon 1}H$ to Thr22 side chain hydroxyl hydrogen bond that would stabilize the helical structure via this very long-range tertiary contact.

Of the positions whose $\Delta\delta^*_{O_2}$ reveals protection within the U_{exch} state, residues 21, 22, 24, and 27 correspond well to the predicted non-native α-helix in the U_{exch} state. Of the remaining protected residues, NOE contacts have been previously identified between the aromatic cluster associated with Trp36 and Tyr37 to Ser34, Ile4, and Ser50.[39,41] Further NOE contacts have been established between Thr12 and Phe9 and between Ile24 and Leu28,[39,41] which are also corroborated by the above normalized shift data. The Arg38 backbone amide has previously been shown to exhibit a number of key long-range NOEs to various regions of the protein in the U_{exch} state[39,41] in addition to exhibiting slow hydrogen exchange. Mutation of Ser10 to Cys and introduction of a spin label in this position caused severe broadening of the majority of the U_{exch} signals in the NMR spectrum, which is indicative of the involvement of Ser10 or nearby residues in a buried structure (J. Marsh and J. Forman-Kay, unpublished results). Our O_2 paramagnetic shift data for Phe9, Thr12, and Ala13 show that these residues are protected from the solvent. Furthermore, both C_α and C_β atoms of Thr12 are protected, with the Cα atom experiencing the smallest shift of all in the U_{exch} state comparable only with the paramagnetic shift of the C_α of Lys21.

The normalized shifts associated with the U_{exch} state would be optimally visualized by mapping $\Delta\delta^*_{O_2}$ onto the surface of several significantly populated conformers of the U_{exch} state if a truly representative ensemble existed. In the absence of this, we have attempted to obtain structures representing the U_{exch} state of the drkN SH3 domain. Our extensive experimental characterizations of the drkN SH3 domain U_{exch} state have led us to develop the program ENSEMBLE[60] for performing structural computations of disordered states of proteins. ENSEMBLE works by assigning population weights to structures in a pregenerated conformer pool in order to calculate an ensemble of structures that collectively are most consistent with experimental observations. Although this approach does not generate a uniquely defined ensemble, we have been able to

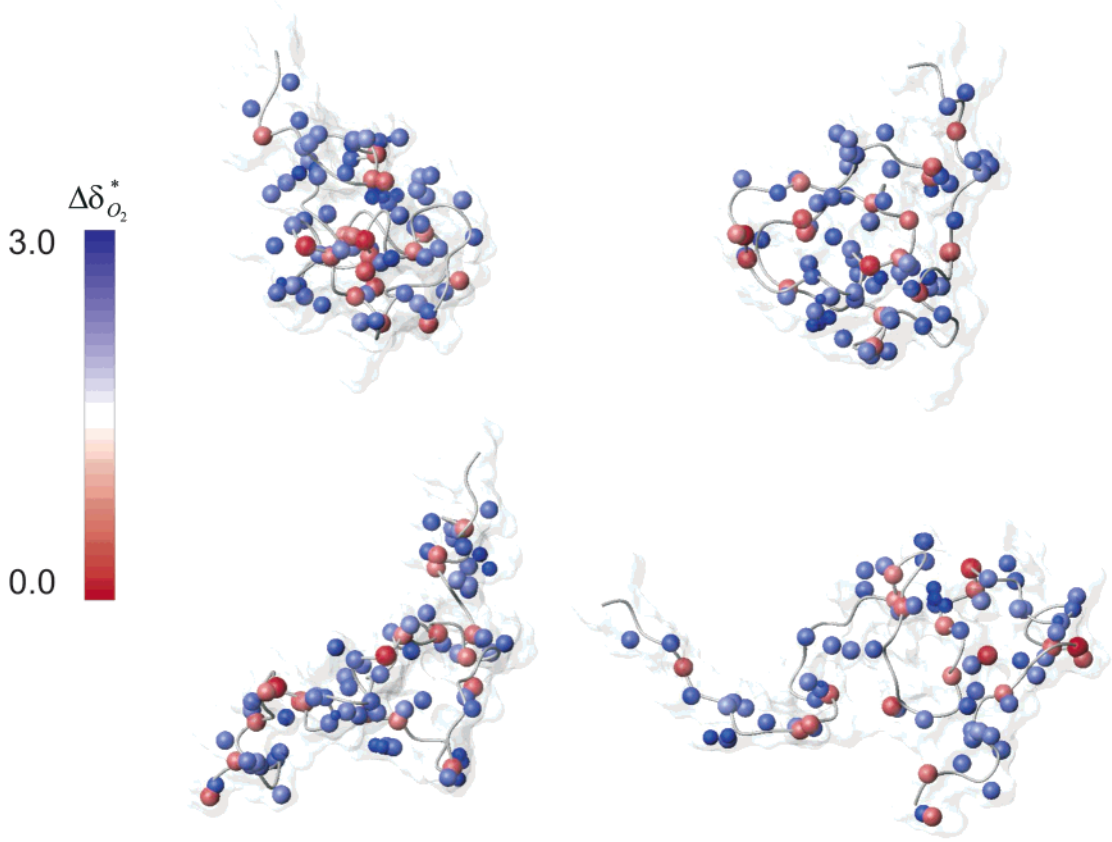

Figure 5. Normalized ^{13}C paramagnetic shifts, $\Delta\delta^*_{O_2}$, for the U_{exch} state, mapped onto four potential structures sampled within the unfolded state ensemble that are consistent with the protection data. Shifts range from red (least solvent exposed) to blue (most exposed). A van der Waals surface is overlaid on each conformer to help distinguish solvent exposed or protected regions.

generate structures that are illustrative of dominant conformers within the drkN U_{exch} state (see Materials and Methods for details).[60,61] This has allowed us to visualize the normalized contact shifts associated with the U_{exch} state by mapping them onto the surfaces of some calculated U_{exch} state conformers. Of the 10 compact structures calculated, four have been highlighted for their consistency with the oxygen paramagnetic shift data. The conformers indicated in the upper row of Figure 5 reveal distinct local clusters of atoms previously identified as being protected from the solvent in the U_{exch} state (i.e., designated as red). The conformers in the lower row of Figure 5 are less compact although the solvent protected atoms appear to lie more on the protein interior in the majority of the cases. We are currently hoping to utilize this oxygen paramagnetic shift data within our ENSEMBLE approach in order to calculate improved U_{exch} state ensembles.

Conclusions and Final Remarks

This paper presents a straightforward approach to the determination of solvent protection and exposure using ^{13}C NMR paramagnetic shifts arising from dissolved oxygen. Via $^1H-^{13}C$ HSQC spectra under unoxygenated and oxygenated conditions, ^{13}C NMR paramagnetic shifts arising from dissolved oxygen were readily observed at 30 and 60 atm partial pressures. The approach is useful in the study of the fluctuating structure of intrinsically disordered protein regions.[1,2,5,6,62,67−69] The paramagnetic ^{13}C shifts arising from dissolved oxygen are ideal probes of local clustering, solvent protection, and hydrophobicity. Such information, particularly when obtained over the entirety of the protein backbone and side chains, is useful in NMR studies of protein folding or unfolding or in studies of disordered proteins for which structural data are generally limited.

In this study the folded (F_{exch}) and compact unfolded (U_{exch}) states were simultaneously observed for the drkN SH3 domain under nondenaturing buffer conditions, enabling a straightforward comparison, though this is not a prerequisite to the application of the above technique. For purposes of assessing the solvent exposure within a given state, the measured paramagnetic shift can be divided by that observed for the same atom type within the free amino acid. This normalized shift has the advantage that potential differences in preferential oxygen interactions with given carbon atoms or delocalization and polarization effects are factored out, thereby providing a relative measure of exposure to oxygen for each carbon atom. Improved normalized shift values are expected once shift measurements can be made for each amino acid in tripeptides that better approximate the environment of an amino acid in a polypeptide. Additional data can also be obtained by measuring paramagnetic shifts for carbonyl carbons.

The protection data presented here are in agreement with many previous observations regarding structure within the U_{exch} state of the drkN SH3 domain. In addition, it has provided a

(66) Feldman, H. J.; Hogue, C. W. V. *Proteins: Struct., Func., Genet.* **2000**, *39* (2), 112−131.
(67) Uversky, V. N. *J. Biomol. Struct. Dyn.* **2003**, *21* (2), 211−234.
(68) Hansen, J. C.; Lu, X.; Ross, E. D.; Woody, R. W. *J. Biol. Chem.* **2006**, *281* (4), 1853−1856.
(69) Tompa, P. *Trends Biochem. Sci.* **2002**, *27* (10), 527−533.

significant amount of new insight and data for residues about which little information existed. An assumption in our analysis has been that the bulk of oxygen-induced paramagnetic shifts arise simply from the extent of solvent exposure rather than gross differences in hydrophobicity and, consequently, differences in the partitioning of oxygen to such hydrophobic regions. It should be possible to distinguish between local surface free energy and solvent exposure by combining the measurement of paramagnetic effects from oxygen with paramagnetic effects from a dissolved hydrophilic agent.[70] Ideally, contrast effects from dissolved oxygen should be compared with exposure to a hydrophilic contrast agent of similar size. Though water is not paramagnetic, effects from water such as NOEs to ^{15}N- and ^{13}C-bonded protons will be indicative of solvent exposure and thus might complement paramagnetic effects from dissolved oxygen.[71] Our ultimate goal will be to derive pseudopotentials based on solvent exposed surface areas and surface hydrophobicities, such that paramagnetic effects from dissolved oxygen and small hydrophilic paramagnetic complexes, in addition to water NOEs, may be used to quantitatively derive structural information for proteins in general, and for disordered proteins in particular.

Acknowledgment. The authors thank Dr. L. E. Kay for many helpful discussions. This work was supported by grants from the Petroleum Research Council (R.S.P.), NSERC (R.S.P.), and CIHR (J.F.-K.), and a fellowship award from the CIHR Strategic Training Program in Protein Folding (I.B.).

Supporting Information Available: Paramagnetic shifts, $\Delta\delta_{O_2}$, and normalized paramagnetic shifts, $\Delta\delta^*_{O_2}$, for F_{exch} and U_{exch} states of the drkN SH3 domain in the presence of dissolved oxygen at a partial pressure of 60 atm (Table S1), as well as the difference between paramagnetic shifts, $\Delta\Delta\delta_{O_2}$, for F_{exch} and U_{exch} states of the drkN SH3 domain in the presence of dissolved oxygen at a partial pressure of 60 atm (Table S2). This material is available free of charge via the Internet at http://pubs.acs.org.

JA065173O

(70) Teng, C. L.; Bryant, R. G. *J. Magn. Reson.* **2006**, *179* (2), 199−205.
(71) Evanics, F.; Hwang, P. M.; Cheng, Y.; Kay, L. E.; Prosser, R. S. *J. Am. Chem. Soc.* **2006**, *128* (25), 8256−8264.